Published in final edited form as:

IEEE Trans Ultrason Ferroelectr Freq Control. 2015 December ; 62(12): 2031–2042. doi:10.1109/TUFFC.2014.006882.

In Vivo Application and Localization of Transcranial Focused Ultrasound Using Dual-Mode Ultrasound Arrays

Alyona Haritonova [Student Member, IEEE],
Department of Biomedical Engineering, University of Minnesota Twin Cities

Dalong Liu [Member, IEEE], and
Department of Electrical and Computer Engineering, University of Minnesota Twin Cities

Emad S. Ebbini [Fellow, IEEE]
Department of Electrical and Computer Engineering, University of Minnesota Twin Cities

Alyona Haritonova: harit005@umn.edu; Dalong Liu: liuxx293@umn.edu; Emad S. Ebbini: emad@umn.edu

Abstract

Focused ultrasound (FUS) has been proposed for a variety of transcranial applications, including neuromodulation, tumor ablation, and blood brain barrier opening. A flurry of activity in recent years has generated encouraging results demonstrating its feasibility in these and other applications. To date, monitoring of FUS beams have been primarily accomplished using MR guidance, where both MR thermography and elastography have been used. The recent introduction of real-time dual-mode ultrasound array (DMUA) systems offers a new paradigm in transcranial focusing. In this paper, we present first experimental results of ultrasound-guided transcranial FUS (tFUS) application in a rodent brain, both *ex vivo* and *in vivo*. DMUA imaging is used for visualization of the treatment region for placement of the focal spot within the brain. This includes the detection and localization of pulsating blood vessels at or near the target point(s). In addition, DMUA imaging is used to monitor and localize the FUS-tissue interactions in real-time. In particular, a concave (40-mm radius of curvature), 32-element, 3.5 MHz DMUA prototype was used for imaging and tFUS application in *ex vivo* and *in vivo* rat model. The *ex vivo* experiments were used to evaluate the point spread function (psf) of the transcranial DMUA imaging at various points within the brain. In addition, DMUA-based transcranial ultrasound thermography measurements were compared with thermocouple measurements of subtherapeutic tFUS heating in rat brain *ex vivo*. The *ex vivo* setting was also used to demonstrate the DMUA capability to produce localized thermal lesions. The *in vivo* experiments were designed to demonstrate the ability of the DMUA to apply, monitor, and localize subtherapeutic tFUS patterns that could be beneficial in transient blood brain barrier opening. The results show that, while the DMUA focus is degraded due to the propagation through the skull, it still produces localized heating effects within sub-millimeter volume. In addition, DMUA transcranial echo data from brain tissue allow for reliable estimation of temperature change.

I. Introduction

The use of FUS for targeting fine structures within the central nervous system (CNS) goes back to the 1950s with the pioneering work reported by Prof. William Fry and colleagues at the University of Illinois [1]– [5]. Francis J. Fry and co-workers published results from

several *ex vivo* and *in vivo* studies investigating and demonstrating the feasibility of localized application of “transkull” ultrasound [6]–[9]. In [9], for example, they have demonstrated that intense, 1-MHz focused ultrasound beams, through a formalin-fixed human skull overlay, produced lesions in (craniectomized) cat brain *in vivo*. These lesions were characterized as having the histological appearance of lesions produced without the human skull overlay. These results lent strong support to the idea of performing a range of therapeutic and subtherapeutic applications of transcranial focused ultrasound (tFUS), including neuromodulation, tumor therapy, epilepsy, etc. However, the lack of reliable, real-time image guidance of tFUS continued to be a challenge, which hindered the progress toward the many significant clinical applications that awaited at the time.

Advances in diagnostic imaging and real-time image guidance methods, especially MRI, renewed interest in tFUS applications. Hynynen and co-workers [10], [11] and Fink and co-workers [12], [13] have investigated numerical methods for transcranial focusing of ultrasound with experimental demonstrations. These efforts, and those of other groups, have demonstrated the feasibility of transkull focusing when accurate CT or MR imaging is available to account for distortions through the skull. In addition, research on opening of the blood brain barrier using FUS has exploded in recent years (e.g. [14]–[29]), mostly in rodent *in vivo* models and utilizing ultrasound contrast agents. Furthermore, the work of Tyler and co-workers [30], [31] has also renewed interest in neuromodulation using tFUS [32]–[37].

A critical review of the majority of the publications on tFUS show that either the FUS transducer or the monitoring technique or both are lacking the localization of the therapeutic effect. This does not lessen the significance of the findings and conclusions of these studies. However, it may present an obstacle towards more complete understanding of the FUS-tissue interactions leading to the desired therapeutic endpoint for a given treatment. This is especially important in small-animal pre-clinical models widely used in brain research. While it is generally accepted that the beam distortion through the mouse skull is minimal at a range of frequencies, it is not the case for larger animals including rats [38].

To address the feedback and localization issues, we have designed and began an experimental validation study of a new dual-mode ultrasound array (DMUA) system for forming, monitoring, and characterization of subtherapeutic pulsed tFUS fields in the *in vivo* rat model. In this paper, we present both *ex vivo* and *in vivo* results that demonstrate the capabilities of the DMUA in image-guided placement of tFUS beams as well as monitoring their interactions with brain tissue. The results shown provide experimental validation of the ability of DMUA imaging to capture important landmarks to allow targeting specific regions within the brain. In addition, we present experimental results demonstrating the use of DMUA-based, real-time transcranial ultrasound thermography (UST) in monitoring and localizing the thermal response to subtherapeutic application of tFUS. The UST estimation is validated using thermocouple measurements in *ex vivo* experiments. Transcranial *in vivo* UST data obtained before, during and after tFUS clearly demonstrate the localized nature of the heating patterns.

II. Methods

A. Dual-Mode Ultrasound Array System

The DMUA prototype (Imasonic, Voray sur l'Ognon, France) shown in Figure 1 was used to obtain the results shown in this paper. Figure 1(a) shows the physical enclosure with array aperture defined by the dark-colored region. Figure 1(b) shows a schematic representation of the array geometry. The array has 32 elements on a spherical shell with a 40-mm radius of curvature. The array elements linearly sampled a 60° aperture opening in the lateral (x) direction with a center-to-center spacing of 1.4 mm. The array aperture in the elevation (y) direction was approximately 45°. An axial line connecting the apex of the array and the geometric center is shown. Figure 1(b) also provides a visualization of the skullcap's position with respect to the DMUA. The coordinates of the skullcap (shown as a wire mesh) are typical for the experiments described below. The figure also shows the intensity profile of the DMUA geometric focus in a homogeneous medium. Compared to the system described in [39], our system has higher focusing gain and smaller focal spot, which is beneficial in terms of minimizing the collateral damage in and around the skull.

1) DMUA Imaging Modes for Guidance and Monitoring—The DMUA was used in synthetic-aperture (SA) imaging mode for guidance and in single-transmit-focus (STF) mode for monitoring. These imaging modes are described in [40] and [41].

Image Guidance: SA imaging employs focusing on both transmit and receive for every pixel providing the highest possible contrast and dynamic range [41]. For the DMUA prototype described in this paper, each imaging frame requires 32 different transmissions; one transmit element and 32 simultaneous receiving elements. Our system currently supports real-time SA frame rates of approximately 30 frames per second (fps). The limitation is due to the use of a gigabit Ethernet to upload the element data for processing by the GPU-based beamformer [42].

The point spread function of SA imaging was evaluated numerically [41] and experimentally [42]. A fractional bandwidth of 50% was used for the simulation (based on data from the manufacturer and testing in our laboratory). A center frequency of 3.5 MHz was assumed in the simulation. The axial 6-dB resolution was equal to 340 μm while the lateral resolution was equal to 280 μm. The corresponding measured values in water tank using a 50-μm wire were 440 μm axial and 352 μm lateral.

We have also characterized the imaging field of view (*FoV*) [40] of the DMUA, which is the region around the geometric focus where SA imaging produces spatially-accurate, high-contrast maps of the object. The FoV for this DMUA extends by ±10 mm and ±8 mm in the axial and lateral dimensions, respectively. Outside this region, grating lobe effect significantly reduces the image contrast.

Monitoring of tFUS Using STF-based Thermography: STF imaging utilizes a single-transmission per frame, where focused transmit beam is used (with dynamic receive beamforming). The advantages of this mode in image-guided FUS applications are described in [40], [42], [43]. The element excitations in STF mode are sub-microsecond

pulses (0.75 - 2 cycles) at the center frequency of the transducer. The delay profiles are typically obtained from the phases of the tFUS beam being monitored. This allows for the characterization of tFUS-tissue interactions, e.g. characterize the reflections from the scalp and skull. Up to 1000 fps can be supported in real-time STF mode using our existing DMUA system. This is sufficient to capture the fast tissue deformation dynamics, including breathing, pulsations and mechanical responses to the acoustic radiation force effects of tFUS. When tFUS is applied, STF frame rates of 400 fps are used to minimize the corruption of the imaging data by reverberations from the therapy bursts.

In this paper, STF was used to obtain ultrasound thermography images before, during, and after the application of subtherapeutic tFUS beams. The GPU-based realtime UST algorithm described by Liu and Ebbini [44] was modified to use with the DMUA prototype instead of a diagnostic ultrasound probe. The results shown in this paper are obtained using the imaging equation given in the Appendix (Eq. 4). As in our previous formulation in [45], the temperature change depends on the local values of the speed of sound (c_0) and its thermal coefficient (β), together with the coefficient of thermal expansion (α). In addition, the imaging equation depends on a parameter (y_0) that accounts for the spatial memory of the temperature rise. For brain tissue, we used $c_0 = 1520$ m/s, $\beta = 1 \times 10^{-3}$ °C^{-1}, and $\alpha = 1.21 \times 10^{-4}$ °C^{-1}. The parameter y_0 is chosen to control the bandwidth of the recursive echo strain filter (RESF) [46]. The choice of y_0 affects both the bandwidth and the gain of the RESF and needs to be accounted for when making quantitative temperature imaging measurements based on (4).

Strain Imaging: Note that the second term in the RESF imaging equation (4) is a discrete-space approximation of an axial derivative operator of the echo shifts. This derivative operator is also used in our original formulation of UST, which we refer to as the infinitesimal echo strain filter. Therefore, the estimation of temperature change is similar to the strain imaging problem [45]. Other authors have recognized the similarity between UST processing and elastography [47], [48].

2) Therapeutic FUS Output—The acoustic output of the DMUA prototype was measured at low driving power levels using an ultrasound power meter (Ohmic Instruments, Easton, MD). Several exposure levels were measured at 0.25, 0.55, 1.0, 1.56, 2.25, 4.0, 6.25, 9 W acoustic. These produced focal intensity values (in water) in the range of 100 - 3500 W/cm^2. The focal intensity values were calculated based on the geometric focusing gain of the concave aperture. Note that the DMUA is capable of producing much higher intensities than these values, but we typically limit our measurements to this range for repeatability. Also, this range was selected based on previous experience in performing subtherapeutic heating in soft tissue. For example, accounting for reflection, attenuation, and defocusing through the skull, a 1-sec, 2.25 W tFUS beam focused at a point 5-mm below the skullcap is expected to produce a focal temperature rise on the order of 1 - 2°C.

We have determined the therapeutic operating field (*ThxOF*) [40] for the DMUA, which is the region around the geometric focus where the focusing gain is within 3-dB of the maximum focusing gain at the DMUA geometric center. Simulation and experimental measurements were consistent and showed that the ThxOF extends by ±2.5 mm axially and

±3 mm laterally. Outside the ThxOF, the focusing gain drops very quickly, limiting the ability of the DMUA to produce localized therapeutic effects at the desired focus location.

B. Ex Vivo Studies

1) Spatial Resolution of Synthetic-aperture DMUA Imaging—For the resolution study, the skull of the animal was transected in the coronal plane with a bone saw (Mar-Med Inc., Cleveland, OH). Opening of the skull allowed an open access to the brain, where five segments of 50 μm wire were inserted orthogonal to the DMUA imaging plane to serve as point targets. The locations of these are shown in Figure 2(a). The transected plane was mounted on a holder attached to a 3D servomotor positioning system with the skullcap facing the DMUA as shown in Figure 2(b).

Spatial Compounding of SA Imaging: Due to the limited FoV of SA images, spatial compounding was used to obtain images with multiple targets. Five SA images were acquired to represent the 5-wire target shown in Figure 2(a). Each SA image was acquired with one of the wires appearing approximately at the geometric center of the DMUA. This was accomplished by positioning the sample in front of the DMUA as in Figure 2(b) and moving it laterally. The central wire was visible in all five images appearing at approximately (−5, 40), (−2.5, 40), (0, 40), (2.5, 40), (5, 40) mm in each of the five acquired images. Please note that the SA images were formed on a rectilinear grid. The composite image allows for a visual comparison of the DMUA point spread functions at several locations.

2) Characterization of tFUS Heating Localization—Subtherapeutic tFUS shots were used to target different locations within the brain with and without thermocouple (T/C) reference measurements. A 200-μm T-type copper-constantan thermocouple (Omega, Stamford, CT) was inserted through the transected brain and was easily visible on SA imaging. The 3D servomotor stage was used to locate the thermocouple junction (in the elevation direction) by selecting the position that produced the maximum heating rate due to a short tFUS pulse.

Once the thermocouple junction location was determined, two different experiments were performed:

i. *Profiling the tFUS Beam:* Six 1-sec tFUS shots were generated at the geometric center (40-mm axially and 0-mm laterally). Each shot was delivered while the T/C and the brain were moved to a different location around the intended focus (200μm between points). This test measured how sharp is the drop in heating rate in the vicinity of the target point (in both axial and lateral dimensions).

ii. *Bracketing the tFUS Heating Rate:* The T/C was positioned in the vicinity of the tFUS focal spot to minimize the viscous [49] heating while maintaining the sensitivity to the local heating. Five different power settings were used with the same exposure duration for each shot. The focus location was the same for each shot. STF imaging frames were collected synchronously with T/C measurements for each shot. Ultrasound thermography was used to estimate the temperature

change at the expected tFUS focal spot for each exposure. This test serves to compare the sensitivity of DMUA-based UST to thermocouple measurements as well as providing a calibration for expected temperature rise during planned *in vivo* experiments where T/C measurements cannot be used.

Calibration of UST Estimates: The echo shift temperature imaging models leading to Equation 4 or its predecessor in [45] have been validated in phantom studies and *ex vivo*. However, there is a need for spatial filtering to minimize the tissue motion and deformation artifacts *in vivo*. The filtering can be carefully designed to maintain the spatial information, but the estimated temperature values will change. The changes depend on the bandwidth of the filter as well as the underlying raw temperature distribution. In this case, calibration of the peak temperature change may be necessary. The thermocouple experiments described in this section provided a means to calibrate the UST estimates *in vivo*. One calibration factor was obtained from one exposure and applied to all other exposures.

3) Lesion Formation—Therapeutic doses of tFUS were delivered in sacrificed animals (normal animals from different procedures) with the aim of establishing the volumetric extent of typical tFUS-induced lesions produced by the 3.5-MHz DMUA. All procedures were completed within five hours from the time of death. The experiment setup was similar to that shown in Figure 2(b). In this case, however, the whole head with the intact skull and brain was used. Therapeutic tFUS was delivered through the skullcap.

The exposure level and/or duration was varied for therapeutic shots delivered in the left hemisphere under SA image guidance. In addition, three shots were delivered in each treatment plane (40 mm axially, -2, 0, 2 laterally) by electronic focusing. Two minutes of cooling time was allowed between individual shots. STF imaging was used to monitor the tissue response to tFUS before, during, and after lesion formation (at 400 fps). The right hemisphere served as the control.

4) Histological Evaluation—Histological Evaluation: After the lesion formation experiment, the brain was removed and processed for paraffin embedding. Five-micrometer sections taken at 300-micrometer intervals in the horizontal plane were stained with hematoxylin and eosin (H&E). Histological evaluation was then performed by a certified neuropathologist.

C. In Vivo Studies

Three *in vivo* experiments in three different animals were performed under IACUC approved protocol (ID# 1401-31222A) to establish the DMUA capability to target and produce localized subtherapeutic heating under image guidance. A water bolus was used to couple the DMUA to the subject as shown in Figure 3.

The animals were given an intra muscular injection of Ketamine 9-10 mg and Xylazine 1 mg per 275-299 gram rat. Each animals was prepped for the procedure by shaving the head with Oster clippers (40 blade) and applying depilatory cream for approximately a minute to remove remaining fine hair. For the duration of DMUA imaging procedure, the rats were sedated using Harvard Apparatus (Harvard Apparatus, Holliston, MA, USA) through

maintained delivery of Isoflurane and oxygen. The animals were placed in a Stereotaxic frame (World Precision Instruments, Inc, Sarasota, FL, USA) (experimental setup is seen in Figure 3(b)). At the time of the procedure, a veterinary technician was responsible for respiration and body temperature monitoring of the animals. In one experiment, heart rate and body temperature measurements were collected using a BIOPAC system (BIOPAC Systems Inc., Goleta, CA, USA).

A typical procedure began with positioning the DMUA under real-time SA imaging guidance so that the skullcap and the base of the skull are visible at 34±2 mm and 45±2 mm axially from the apex of the DMUA. This allows the positioning the ThxOF of the DMUA centrally within the brain tissue between the skull bones. The ThxOF can be adjusted in the axial direction by inflating or deflating the bolus. Mechanical movements of the DMUA (using a servomotor) in the lateral direction allowed for targeting brain tissue more than 3 mm laterally from the median section of the brain.

The subtherapeutic exposure levels tested in the *ex vivo* experiments described above were tested in the first animal with each exposure repeated three times. This allowed us to choose the appropriate exposure level for robust detection and estimation of temperature rise *in vivo*. Electronic steering was used to position the focal spot at the desired target location, e.g. on a pulsating blood vessel as seen on SA and confirmed on STF imaging modes. The exposure duration was fixed at 1 second in all cases, but the location of the focus was varied electronically in the axial and/or lateral direction by up to ±2 mm. Each subtherapeutic tFUS shot was repeated at least twice to establish repeatability.

1) Histological Evaluation—Each animal was survived for three days following the procedure. At the end of the three-day period, they were sacrificed with CO_2 asphyxiation for a duration of 4 - 5 minutes. Following sacrifice, the brain was removed and processed for paraffin embedding. Five-micrometer sections taken at 300-micrometer intervals in the horizontal plane were stained with hematoxylin and eosin. Histological evaluation was then performed by a certified neuropathologist.

III. Results and Discussion

A. Wire Target Imaging

Figure 4(a) shows a composite image formed by compounding 5 SA images, each obtained with one of the wires centered approximately at the geometric center of the DMUA. The five wires embedded within the brain tissue (Figure 2(a)) are clearly visible on the composite SA image. Four of 5 wires produce echogenicity levels approximately 25 dB above the echogenicity of the brain tissue. The lower echogenicity of the microwire at location 4 is probably due to the difficulty in inserting the 50-μm wire and maintaining it orthogonal to the imaging slice (for maximum echogenicity).

To evaluate resolution values at location 1, we examined Figure 4(b) and Figure 4(c). In these two figures, axial and lateral traces through the maxima of the wire echo are displayed. Figure 4(b) depicts axial distance versus echo amplitude, where the wire echo can be easily identified at 40 mm axially. The tissue trace with the wire removed is depicted in red, and

allows for easy evaluation of the wire location. A similar technique can be applied in the lateral dimension. For location 1, the -6 dB axial and lateral resolution values are estimated at 440 μm and 560 μm, respectively. The remainder of the resolution values are summarized in Table I.

The lateral and axial resolution values exhibit some variations that could be attributed to the location of each wire with respect to the skullcap and the effective angle of entrance of the imaging beams. These issues will be addressed in future reports, together with refocusing methods to restore resolution. It should be noted, however, that the level of variation still allows us to claim sub-millimeter spatial resolution of the system in both axial and lateral dimensions. Therefore, while we expect the focusing capabilities to improve, the current values allow for sub-millimeter precision in placing the tFUS focal point within the brain based on anatomical markers such as skullcap and base of the skull.

B. Characterization of tFUS Heating

The T/C measurements serve to characterize the spatial extent of the heating pattern and provide ground truth for calibrating the DMUA-based ultrasound thermography data obtained using STF imaging. To achieve these goals, we inserted the needle thermocouple into the brain in a similar manner to the wire resolution targets used earlier. The T/C can be easily seen on DMUA SA imaging as demonstrated by Figure 5(a). The colored dots indicate the locations of the tFUS focal spots with respect to the T/C junction. The T/C measurements were obtained during five tFUS shots with the same exposure parameters. For each shot the T/C junction was slightly moved to demonstrate how sharp is the drop off in temperature from the center of heating. This is demonstrated by the T/C temperature profiles shown in Figure 5(b). This result shows the localization of the tFUS heating pattern, especially in the lateral dimension.

With the T/C junction in place very close to the tFUS focal spot indicated by the blue dot, a series of subtherapeutic tFUS shots were repeated at the same location with acoustic power output of 0.25, 1.0, 2.25, 4.00, and 6.25 W and duration of 1 second each. The transcranial DMUA-based estimates of temperature change are shown in Figure 5(c) and the corresponding T/C measurements are shown in Figure 5(d). The main difference between the two measurements is the sharper initial heating and sharper initial decay in the T/C measurements compared to the UST profiles. This is possibly due to a small viscous heating component resulting from the proximity of the T/C to the focal point of the tFUS beam. The exponential rise on the DMUA temperature is better highlighted when the thermocouple does not interfere with the focal beam. Based on these *ex vivo* results, we decided to limit the subtherapeutic exposure *in vivo* to the range of 1 - 2.25 W. These exposures were high enough to produce temperature rise above the baseline while being low enough to minimize adverse effects in the live subjects.

C. Transcranial Lesion Formation

Figure 6 shows an example thermal lesion formed using the DMUA to generate a 1-sec tFUS shot at an acoustic power output of 49 W. This output level is approximately 3 times

the output needed to form a lesion in soft tissue (without the skull in the path of the FUS beam).

Histological examination of the brain tissue revealed a single lesion located on the left side of the brain, as seen in Figure 6(a). The cells appeared thermally coagulated, and a sharp transition was observed from coagulated to normal tissue. A more detailed depiction of the lesion is seen in Figure 6(b), where the perimeter of the lesion is outlined with a red marker. The diameter of the lesion cross-section was measured at 689 μm. The lesion was visualized in two axial histological slices, thus the approximate height of the lesion was less than 900 μm. The control region captured in Figure 6(c) did not reveal the presence of coagulated or compromised cells.

It should be noted that other therapeutic tFUS shots were attempted in the left hemisphere of the same brain, but there was no evidence of damage other than the lesion shown. Nonetheless, this result provides additional evidence of the high degree of localization of transcranial focusing achieved using this DMUA prototype.

D. Transcranial Imaging and Subtherapeutic Focusing In Vivo

An important goal of this study is to establish that subtherapeutic tFUS can be delivered safely and repeatably under DMUA imaging guidance. An equally important goal is to demonstrate the reliability and repeatability of STF-based ultrasound thermography as a form of feedback for monitoring and localizing the thermal response to subtherapeutic tFUS.

Figure 7 shows the results from the *in vivo* application of subtherapeutic tFUS in the brain of Rat A. The objective was to bracket the tFUS exposure at a point within the brain. The target was at an axial distance of 40 mm and lateral distance of 0 mm. The SA image in Figure 7(a) shows a strong reflection just above the target point. A typical spatial temporal temperature profile obtained using our UST method to STF data is shown in Figure 7(b) (2.25 W acoustic power). This result shows pronounced heating and decay pattern between 37 - 39 mm in the axial direction. The temperature rise and peak are consistent with the tFUS ON and tFUS OFF times (at 1 second and 2 seconds, respectively). The spatial temporal pattern also reveals the presence of a pulsating artery at an axial distance of 42 mm above the base of the skull. The pulsation was recognizable and localized on SA imaging (15 fps). When using STF imaging, it was easily recognizable and was consistent with the heart rate in the rat (approximately 180 beats per minute in this case). This type of measurement was confirmed in the Rat C experiment, where the ECG was directly measured.

The spatio temporal map in Figure 7(b) shows a slight increase of temperature within the scalp (≈33 mm). The maximum temperature within the scalp was less than 0.25°C with a rise and decay profile similar to the focal heating (at ≈ 38 mm.) We note that the time between tFUS shots was 2 minutes to allow temperature rise to go back to baseline before each new tFUS shot.

Figure 7(c) shows the result of bracketing the subtherapeutic tFUS exposure for the five levels of exposure (0.25, 0.55, 1, 1.56, 2.25 W). As with the *ex vivo* case shown earlier, the

lowest exposure level did not yield a reliable estimate of the temperature rise while the other showed a measurable rise above the baseline. Each of these was repeated three times and the shown profiles reflect the procedure, i.e. 0.25 W X1, 0.55 W X1, 1 W X3, 1.56 W X3, and 2.25 W X3. The standard deviation for each trace is indicated by the bars. The repeatability of the measurement is well demonstrated by the 1 W and 2.25 W exposures, while a higher level of variation was observed for the 1.56 W exposure.

Figure 8 shows the results from the *in vivo* application of subtherapeutic tFUS in the brain of Rat B. The objective was to test electronically steered tFUS patterns. The target was at an axial distance of 40 mm and lateral distance of -1 mm. The SA image in Figure 8(a) shows a strong reflection just above the target point. A typical spatial temporal temperature profile obtained using our UST method to STF data is shown in Figure 8(b). This result shows localized heating and decay pattern between 37 - 39 mm in the axial direction as in the previous case. However, the heating rate at this location is lower. Some artifacts can also be seen in the spatial temporal profile. For example, apparent temperature changes in the scalp (≈33 mm) and just below the cranium floor (≈45 mm) can be seen. These changes may be related to the tFUS, but their temporal profile is not indicative of temperature rise. These types of artifacts usually appear in boundary regions with low echogenicity where sensitivity to motion is quite high. In this case, they appear to reflect a change in the pulsation pattern in response to the application of tFUS. We have developed compensation algorithms for these types of artifacts that could be applied to improve the UST results [46]. It should be noted, however, that the artifacts do not obscure the localized heating produced by the tFUS beam near the intended target.

For Rat B (and subsequent experiments), we only applied a small number of subtherapeutic tFUS shots to minimize the possibility of creating unintended damage in the brain. In this case, we applied 3, 1-second tFUS shots focused at -1 mm laterally and 40 mm axially. The 1 W shot produced a measurable temperature rise, but the 1.56 W shot was deemed more reliable and was repeated twice. The traces in Figure 8(c) demonstrate the temperature rise and decay consistent with the application of the tFUS shots.

The results from Rat C (three 1-sec tFUS shots at 2.25 W, focused at 39 mm axially and 0 mm laterally) exhibited similar behavior to the examples shown from rats A and B. These results are not shown here to avoid repetition.

To summarize, subtherapeutic tFUS heating in three rats resulted in localized estimated temperature rise approximately 1 - 2 mm above the target heating point. Temperature imaging artifacts did not obscure this focal temperature rise in any of the *in vivo* heating experiments with acoustic power levels in the 1 - 2 W range. Furthermore, the estimated heating rates *in vivo* are in agreement with the heating rates measured *ex vivo* and confirmed using reference thermocouple measurements.

Post-treatment Evaluation—Upon completion of the experiment all animals fully recovered from the anesthetic and exhibited normal behavior with no apparent loss of physiological function. The histological examination of the brain tissue also confirmed lack of cellular damage in all three animals. Furthermore, the ECG signal monitored on one of

the animals did not exhibit abnormal changes during or after the application of subtherapeutic tFUS procedures. All of these observations support the notion that subtherapeutic tFUS resulting in localized, mild increase in temperature for 1 second appears to be safe, even when repeated at one or more locations within the brain of the rat model.

E. Monitoring Pulsations Using STF

Finally, we show examples to demonstrate the ability of our DMUA imaging to detect and localize pulsations at relatively high frame rates. Figure 9 shows two different instances of pulsation. The first was observed while delivering a subtherapeutic tFUS shot. A strong pulsation signature was visualized below the cranium floor. Initially, the effect was visualized at 400 fps, and as seen on Figure 9(a), the strain computed using the UST algorithm is representative of the arterial pressure curve (see Figure 9(d)). Increasing the frame rate to 1000 fps enabled us to visualize a greater degree of detail as seen on Figure 9(e). Here the diastolic notch is apparent on each pulsation cycle. Three pulsation cycles that have been observed are representative of the heart rate of the animal, which was estimated at approximately 180 beats per minute. In addition to transcranial pulsation imaging, imaging of the chest cavity was also performed for additional confirmation. Figure 9(c) depicts axial-temporal dynamics of a beating heart. The image was obtained by positioning DMUA on the spine of the animal. Strain dynamics seen on Figure 9(f) are representative of a wall of a ventricle in a rat. These results demonstrate the capability of the DMUA imaging to identify, localize and track physiological signals that could be useful in image-guided interventions. For example, these sources of physiological signals could be targeted or avoided by adaptive beamforming of DMUA tFUS patterns [43]. Furthermore, the physiological signals could provide a reliable source of triggered tFUS in some applications.

IV. Conclusion

The feasibility of real-time image-guided placement and monitoring of tFUS beams using dual-mode ultrasound arrays was demonstrated in a rat model. Synthetic aperture DMUA imaging was shown to reliably capture key anatomical features delineating the scalp, skull and the base of the skull. Furthermore, pulsating arteries within the *FoV* are often detectable on SA imaging. This is significant since vessels are often the target of potential transcranial therapies. The results shown in this paper have also demostrated that real-time transcranial ultrasound thermography *in vivo* is capable of detecting and localizing the subtherapeutic tFUS heating profile with high spatial and temporal resolution. The heating rates estimated *in vivo* were consistent with those measured *ex vivo* using thermocouples during the application of subtherapeutic tFUS patterns with similar acoustic power outputs. Some artifacts were observed on spatio-temporal temperature change profiles, but they neither obscured the actual heating pattern nor limited our ability to localize the tissue response to tFUS. These preliminary findings are likely to be further strengthened by the application of planned adaptive refocusing for improved transcranial imaging and therapy with DMUAs. Not only will the DMUA approach provide a means to guide the placement of tFUS beams, it will also provide a highly specific imaging to characterize the tFUS-tissue interactions. This could be the key to better understanding of the mechanisms at play in major

applications like neuromodulation, blood-brain barrier opening, and enhanced delivery of therapeutic agents.

Acknowledgments

We are indebted to Dr. Andrew J. Casper for outstanding design of receiving circuitry and real-time implementation of GPU-based beamdforming. Dr. H. Brent Clark, MD, PhD (Professor of Laboratory Medicine and Pathology, Neurology, and Neurosurgery, University of Minnesota Medical School) provided detailed comments on the histology results from the lesion formation *ex vivo* and subtherapeutic tFUS *in vivo* experiments. He also revised the final description of the histology results presented in this paper. We are grateful for his help and advice. We thank Ms. Colleen Forster for her work on the histology slides. We would like to thank Ms. Juan Du and Mr. Fei Zheng for their assistance during the experiments. Dr. John Ballard, Dr. Mahdi Bayat and Mr. Elias Wilken-Resman also assisted with the initial SA *ex vivo* imaging. We gratefully acknowledge the excellent dedication in caring for the animals by Ms. Brenda Koniar and Ms. Meri DuRand from Research Animal Resources at UM.

Funded in part by grant NS087887 from the National Institutes of Health and in part by the University of Minnesotas MnDRIVE (Minnesotas Discovery, Research and Innovation Economy) initiative.

Appendix A

For pulse-echo imaging, the two-way delay of the echo from a scatterer located at depth y is given by:

$$\tau(y;\theta)=2\int_0^y \frac{d\xi}{c\,(\xi;\theta)} \quad (1)$$

where $\theta(\xi) = \theta_0 + \delta\theta$ is the temperature profile along the beam trajectory assumed to deviate infinitesimally from the baseline temperature θ_0. Using this infinitesimal change model, we can express the speed of sound as:

$$c\,(z;\theta\,(y)) = c_0\,(y)\,[1+\beta\,(y)\,\delta\theta\,(y)] \quad (2)$$

where $\beta(y)$ is the thermal coefficient of the speed of sound given by

$$\beta(y)=\frac{1}{c_0(y)}\cdot\frac{\partial c\,(y;\theta)}{\partial\theta}\Big|_{\theta=\theta_0} \;\&c_0(y)=c(y;\theta_0). \quad (3)$$

Accounting for thermal expansion by modifying the limit of the integral in (1) [46], a recursive discrete-space filter was derived to compute the frame-to-frame temperature change from the spatial tissue displacement profile in the axial direction:

$$\delta\theta\,(y_i) = a\cdot\delta\theta\,(y_{i-1}) + b\cdot(\delta\tau\,(y_i) - \delta\tau\,(y_{i-1})) \quad (4)$$

$$a=\frac{\alpha\tau - T_s\,(\alpha+\beta)}{\alpha\tau+T_s\,(\alpha+\beta)} \quad b=-\frac{2T_s}{\alpha\tau+T_s\,(\alpha+\beta)}$$

where α is the coefficient of thermal expansion, T_s is the echo sampling period, and $\tau = 2y_0/c_0$ is a parameter that defines the extent of the spatial memory of the recursive filter. This filter, referred to as the recursive echo strain filter (RESF) in [46], accounts for a nonuniform temperature baseline when computing the spatial temperature change between two frames. This is a major difference from our previously proposed infinitesimal echo strain filter (δ-ESF) approach described by Simon *et al* [45].

The tissue-dependent parameters in (4) can be accounted for based on known or measured acoustic and thermal properties of the tissue being heated. This algorithm was validated in tissue-mimicking phantoms and in *ex vivo* tissue experiments where these properties can be reliably estimated/measured.

References

1. Fry W, Mosberg JW, Barnard J, Fry F. Production of focal destructive lesions in the central nervous system with ultrasound. J Neurosurgery. 1954; 11:471–478.
2. Barnard JW, Fry WJ, Fry FJ, Brennan JF. Small localized ultrasonic lesions in the white and gray matter of the cat brain. AMA Arch Neurol Psychiatry. Jan; 1956 75(1):15–35.
3. Fry WJ, Barnard JW, Fry EJ, Krumens RF, Brennan JF. Ultrasonic lesions in the mammalian central nervous system. Science. Sep; 1955 122(3168):517–518. [PubMed: 13255886]
4. Meyers R, Fry WJ, Fry FJ, Dreyer LL, Schultz DF, Noyes RF. Early experiences with ultrasonic irradiation of the pallidofugal and nigral complexes in hyperkinetic and hypertonic disorders. J Neurosurg. Jan; 1959 16(1):32–54. [Online]. Available: http://dx.doi.org/10.3171/jns.1959.16.1.0032. [PubMed: 13621264]
5. Wulff VJ, Fry WJ, Tucker D, Fry FJ, Melton C. Effect of ultrasonic vibrations on nerve tissues. Proc Soc Exp Biol Med. Feb; 1951 76(2):361–366. [PubMed: 14827926]
6. Fry FJ. Transkull transmission of an intense focused ultrasonic beam. Ultrasound Med Biol. 1977; 3(2-3):179–184. [PubMed: 595211]
7. Fry FJ, Barger JE. Acoustical properties of the human skull. J Acoust Soc Am. May; 1978 63(5): 1576–1590. [PubMed: 690336]
8. Fry FJ, Goss SA. Further studies of the transkull transmission of an intense focused ultrasonic beam: lesion production at 500 khz. Ultrasound Med Biol. 1980; 6(1):33–38. [PubMed: 7368418]
9. Fry FJ, Goss SA, Patrick JT. Transkull focal lesions in cat brain produced by ultrasound. J Neurosurg. May; 1981 54(5):659–663. [Online]. Available: http://dx.doi.org/10.3171/jns.1981.54.5.0659. [PubMed: 7014793]
10. Sun J, Hynynen K. Focusing of therapeutic ultrasound through a human skull: a numerical study. J Acoust Soc Am. Sep; 1998 104(3 Pt 1):1705–1715. [PubMed: 9745750]
11. Yin X, Hynynen K. A numerical study of transcranial focused ultrasound beam propagation at low frequency. Phys Med Biol. Apr; 2005 50(8):1821–1836. [Online]. Available: http://dx.doi.org/10.1088/0031-9155/50/8/013. [PubMed: 15815098]
12. Aubry JF, Tanter M, Pernot M, Thomas JL, Fink M. Experimental demonstration of noninvasive transskull adaptive focusing based on prior computed tomography scans. J Acoust Soc Am. Jan; 2003 113(1):84–93. [PubMed: 12558249]
13. Marquet F, Pernot M, Aubry JF, Montaldo G, Marsac L, Tanter M, Fink M. Non-invasive transcranial ultrasound therapy based on a 3d ct scan: protocol validation and in vitro results. Phys Med Biol. May; 2009 54(9):2597–2613. [Online]. Available: http://dx.doi.org/10.1088/0031-9155/54/9/001. [PubMed: 19351986]
14. Hynynen K, McDannold N, Vykhodtseva N, Jolesz F. Noninvasive MR imaging-guided focal opening of the blood-brain barrier in rabbits. RADIOLOGY. Sep; 2001 220(3):640–646. [PubMed: 11526261]
15. Alonso A, Reinz E, Leuchs B, Kleinschmidt J, Fatar M, Geers B, Lentacker I, Hennerici MG, de Smedt SC, Meairs S. Focal delivery of aav2/1-transgenes into the rat brain by localized

ultrasound-induced bbb opening. Mol Ther Nucleic Acids. 2013; 2:e73. [Online]. Available: http://dx.doi.org/10.1038/mtna.2012.64. [PubMed: 23423361]

16. Arvanitis CD, Livingstone MS, McDannold N. Combined ultrasound and mr imaging to guide focused ultrasound therapies in the brain. Phys Med Biol. Jul; 2013 58(14):4749–4761. [Online]. Available: http://dx.doi.org/10.1088/0031-9155/58/14/4749. [PubMed: 23788054]
17. Aryal M, Vykhodtseva N, Zhang YZ, Park J, McDannold N. Multiple treatments with liposomal doxorubicin and ultrasound-induced disruption of blood-tumor and blood-brain barriers improve outcomes in a rat glioma model. J Control Release. Jul; 2013 169(1-2):103–111. [Online]. Available: http://dx.doi.org/10.1016/j.jconrel.2013.04.007. [PubMed: 23603615]
18. Burgess A, Ayala-Grosso CA, Ganguly M, Jordo JF, Aubert I, Hynynen K. Targeted delivery of neural stem cells to the brain using mri-guided focused ultrasound to disrupt the blood-brain barrier. PLoS One. 2011; 6(11):e27877. [Online]. Available: http://dx.doi.org/10.1371/journal.pone.0027877. [PubMed: 22114718]
19. Deng CX. Targeted drug delivery across the blood-brain barrier using ultrasound technique. Ther Deliv. Dec; 2010 1(6):819–848. [Online]. Available: http://dx.doi.org/10.4155/tde.10.66. [PubMed: 21785679]
20. Hynynen K. Ultrasound for drug and gene delivery to the brain. Adv Drug Deliv Rev. Jun; 2008 60(10):1209–1217. [Online]. Available: http://dx.doi.org/10.1016/j.addr.2008.03.010. [PubMed: 18486271]
21. Konofagou EE. Optimization of the ultrasound-induced blood-brain barrier opening. Theranostics. 2012; 2(12):1223–1237. [Online]. Available: http://dx.doi.org/10.7150/thno.5576. [PubMed: 23382778]
22. Raymond SB, Treat LH, Dewey JD, McDannold NJ, Hynynen K, Bacskai BJ. Ultrasound enhanced delivery of molecular imaging and therapeutic agents in alzheimer's disease mouse models. PLoS One. 2008; 3(5):e2175. [Online]. Available: http://dx.doi.org/10.1371/journal.pone.0002175. [PubMed: 18478109]
23. Treat LH, McDannold N, Vykhodtseva N, Zhang Y, Tam K, Hynynen K. Targeted delivery of doxorubicin to the rat brain at therapeutic levels using mri-guided focused ultrasound. Int J Cancer. Aug; 2007 121(4):901–907. [Online]. Available: http://dx.doi.org/10.1002/ijc.22732. [PubMed: 17437269]
24. Treat LH, McDannold N, Zhang Y, Vykhodtseva N, Hynynen K. Improved anti-tumor effect of liposomal doxorubicin after targeted blood-brain barrier disruption by mri-guided focused ultrasound in rat glioma. Ultrasound Med Biol. Oct; 2012 38(10):1716–1725. [Online]. Available: http://dx.doi.org/10.1016/j.ultrasmedbio.2012.04.015. [PubMed: 22818878]
25. Tung YS, Vlachos F, Feshitan JA, Borden MA, Konofagou EE. The mechanism of interaction between focused ultrasound and microbubbles in blood-brain barrier opening in mice. J Acoust Soc Am. Nov; 2011 130(5):3059–3067. [Online]. Available: http://dx.doi.org/10.1121/1.3646905. [PubMed: 22087933]
26. Liu HL, Hua MY, Yang HW, Huang CY, Chu PC, Wu JS, Tseng IC, Wang JJ, Yen TC, Chen PY, Wei KC. Magnetic resonance monitoring of focused ultrasound/magnetic nanoparticle targeting delivery of therapeutic agents to the brain. Proc Natl Acad Sci U S A. Aug; 2010 107(34):15 205–15 210. [Online]. Available: http://dx.doi.org/10.1073/pnas.1003388107.
27. Liu HL, Chen PY, Yang HW, Wu JS, Tseng IC, Ma YJ, Huang CY, Tsai HC, Chen SM, Lu YJ, Huang CY, Hua MY, Ma YH, Yen TC, Wei KC. In vivo mr quantification of superparamagnetic iron oxide nanoparticle leakage during low-frequency-ultrasound-induced blood-brain barrier opening in swine. J Magn Reson Imaging. Dec; 2011 34(6):1313–1324. [Online]. Available: http://dx.doi.org/10.1002/jmri.22697. [PubMed: 21965168]
28. Yoshino SI, Fukushima T, Hayashi S, Nonaka M, Ogawa K, Sasaki K, Umemura SI. Effects of focused ultrasound sonodynamic treatment on the rat blood-brain barrier. Anticancer Res. Mar; 2009 29(3):889–895. [PubMed: 19414324]
29. Marty B, Larrat B, Van Landeghem M, Robic C, Robert P, Port M, Le Bihan D, Pernot M, Tanter M, Lethimonnier F, Mriaux S. Dynamic study of blood-brain barrier closure after its disruption using ultrasound: a quantitative analysis. J Cereb Blood Flow Metab. Oct; 2012 32(10):1948–1958. [Online]. Available: http://dx.doi.org/10.1038/jcbfm.2012.100. [PubMed: 22805875]

30. Tufail Y, Yoshihiro A, Pati S, Li MM, Tyler WJ. Ultrasonic neuromodulation by brain stimulation with transcranial ultrasound. Nat Protoc. Sep; 2011 6(9):1453–1470. [Online]. Available: http://dx.doi.org/10.1038/nprot.2011.371. [PubMed: 21886108]
31. Tyler WJ. Noninvasive neuromodulation with ultrasound? a continuum mechanics hypothesis. Neuroscientist. Feb; 2011 17(1):25–36. [Online]. Available: http://dx.doi.org/10.1177/1073858409348066. [PubMed: 20103504]
32. King RL, Brown JR, Newsome WT, Pauly KB. Effective parameters for ultrasound-induced in vivo neurostimulation. Ultrasound Med Biol. Feb; 2013 39(2):312–331. [Online]. Available: http://dx.doi.org/10.1016/j.ultrasmedbio.2012.09.009. [PubMed: 23219040]
33. Deffieux T, Younan Y, Wattiez N, Tanter M, Pouget P, Aubry JF. Low-intensity focused ultrasound modulates monkey visuomotor behavior. Curr Biol. Dec; 2013 23(23):2430–2433. [Online]. Available: http://dx.doi.org/10.1016/j.cub.2013.10.029. [PubMed: 24239121]
34. Younan Y, Deffieux T, Larrat B, Fink M, Tanter M, Aubry JF. Influence of the pressure field distribution in transcranial ultrasonic neurostimulation. Med Phys. Aug.2013 40(8):082902. [Online]. Available: http://dx.doi.org/10.1118/1.4812423. [PubMed: 23927357]
35. King RL, Brown JR, Pauly KB. Localization of ultrasound-induced in vivo neurostimulation in the mouse model. Ultrasound Med Biol. Jul; 2014 40(7):1512–1522. [Online]. Available: http://dx.doi.org/10.1016/j.ultrasmedbio.2014.01.020. [PubMed: 24642220]
36. Kim H, Lee SD, Chiu A, Yoo SS, Park S. Estimation of the spatial profile of neuromodulation and the temporal latency in motor responses induced by focused ultrasound brain stimulation. Neuroreport. May; 2014 25(7):475–479. [Online]. Available: http://dx.doi.org/10.1097/WNR.0000000000000118. [PubMed: 24384503]
37. Mehić E, Xu JM, Caler CJ, Coulson NK, Moritz CT, Mourad PD. Increased anatomical specificity of neuromodulation via modulated focused ultrasound. PLoS One. 2014; 9(2):e86939. [Online]. Available: http://dx.doi.org/10.1371/journal.pone.0086939. [PubMed: 24504255]
38. O'Reilly MA, Muller A, Hynynen K. Ultrasound insertion loss of rat parietal bone appears to be proportional to animal mass at submegahertz frequencies. Ultrasound Med Biol. Nov; 2011 37(11):1930–1937. [Online]. Available: http://dx.doi.org/10.1016/j.ultrasmedbio.2011.08.001. [PubMed: 21925788]
39. Zhang Y, Aubry JF, Zhang J, Wang Y, Roy J, Mata JF, Miller W, Dumont E, Xie M, Lee K, Zuo Z, Wintermark M. Defining the optimal age for focal lesioning in a rat model of transcranial HIFU. Ultrasound Med Biol. Feb; 2015 41(2):449–455. [Online]. Available: http://dx.doi.org/10.1016/j.ultrasmedbio.2014.09.029. [PubMed: 25542495]
40. Ebbini E, Yao H, Shrestha A. Dual-mode ultrasound arrays for image-guided surgery. Ultrasonic Imaging. Apr.2006 28:65–82. [PubMed: 17094688]
41. Wan Y, Ebbini ES. Imaging with concave large-aperture therapeutic ultrasound arrays using conventional synthetic-aperture beamforming. IEEE Trans UFFC. Feb; 2008 55(2):368–383.
42. Casper A, Liu D, Ballard J, Ebbini E. Real-time Implementation of a Dual-Mode Ultrasound Array System: In Vivo Results. Biomedical Engineering, IEEE Transactions on. Oct; 2013 60(10):2751–2759.
43. Ballard JR, Casper AJ, Wan Y, Ebbini ES. Adaptive Transthoracic Refocusing of Dual-Mode Ultrasound Arrays. IEEE Transactions On Biomedical Engineering. Jan; 2010 57(1):93–102. [PubMed: 19651547]
44. Liu D, Ebbini E. Real-time 2-D temperature imaging using ultrasound. IEEE Trans Biomed Eng. Jan; 2010 57(1):12–16. [PubMed: 19884075]
45. Simon C, VanBaren P, Ebbini ES. Two-dimensional temperature estimation using diagnostic ultrasound. IEEE Trans Ultrason, Ferroelect, Freq Contr. Jul.1998 45:989–1000.
46. Bayat M, Ballard JR, Ebbini ES. In vivo ultrasound thermography in presence of temperature heterogeneity and natural motions. IEEE Trans Biomed Eng. Feb; 2015 62(2):450–457. [Online]. Available: http://dx.doi.org/10.1109/TBME.2014.2358075. [PubMed: 25248172]
47. Miller N, Bamber J, Meany P. Fundamental limitations of noninvasive temperature imaging by means of ultrasound echo strain estimation. Ultrasound in Medicine and Biology. 2002; 28:1319–1333. [PubMed: 12467859]

48. Souchon R, Bouchoux G, Maciejko E, Lafon C, Cathignol D, Bertrand M, Chapelon JY. Monitoring the formation of thermal lesions with heat-induced echo-strain imaging: A feasibility study. Ultrasound in Medicineand Biology. 2005; 31:251–259.

49. Morris H, Rivens I, Shaw A, Haar GT. Investigation of the viscous heating artefact arising from the use of thermocouples in a focused ultrasound field. Phys Med Biol. Sep; 2008 53(17):4759–4776. [Online]. Available: http://dx.doi.org/10.1088/0031-9155/53/17/020. [PubMed: 18701773]

Biographies

Alyona Haritonova (S'14) received her B.A. degree (Valedictorian) in physics from St. Catherine University in St. Paul, Minnesota in 2009. She is currently pursuing her Ph.D. in Biomedical Engineering at the University of Minnesota, Minneapolis, MN. Ms. Haritonova's research interests include monitoring focused ultrasound treatment with phased arrays and biological implications of such a treatment. In 2014 Alyona received a MnDRIVE Graduate Fellowship in support of her research on transcranial imaging and therapy with dual-mode ultrasound phased arrays.

Dalong Liu was born in China in 1977. He received his B.Sc. and M.Sc. degrees in biomedical engineering from Zhejiang University, Hangzhou, China, in 2001 and 2004, respectively. He received his Ph.D. degree in biomedical engineering from University of Minnesota, Minneapolis, in 2010. He was a postdoc in Electrical and Computer Engineering in Minnesota from 2010 to 2011. From 2011 to 2013, he worked as a Senior Engineer in Siemens Medical Solutions, USA. He is currently a research assistant professor in Electrical and Computer Engineering at the University of Minnesota.

His research interests are in image-guided high intensity focused ultrasound (HIFU), ultrasound elastography and thermography, ultrasound imaging, and signal processing.

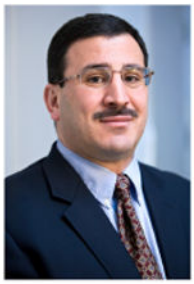

Emad S. Ebbini (S'82, M'90, SM'08, F'11) Received his B.Sc. in EE/communications in 1985 from the University of Jordan, and his M.S. and Ph.D. in EE from the University of Illinois at Urbana-Champaign in 1987 and 1990. From 1990 until 1998, he was on the faculty of the EECS department at the University of Michigan Ann Arbor. Since 1998, he has been with the ECE department at the University of Minnesota. In 1993, he received the NSF Young Investigator Award for his work on new ultrasound phased arrays for imaging and therapy. He was a member of AdCom for the IEEE Ultrasonics, Ferroelectrics, and Frequency Control between 1994 and 1997. In 1996, he was a guest editor for a special issue on therapeutic ultrasound in the *IEEE Transactions on Ultrasonics, Ferroelectrics, and Frequency Control*. He was an associate editor for the same transactions from 1997 - 2002. He is a member of the standing technical program committee for the IEEE Ultrasonics Symposium. He served as a member of the Board of the International Society for Therapeutic Ultrasound (2002 - 2011) and is currently serving as its President (2012 - 2015). His research interests are in signal and array processing with applications to biomedical ultrasound and medical devices.

(a) DMUA enclosure

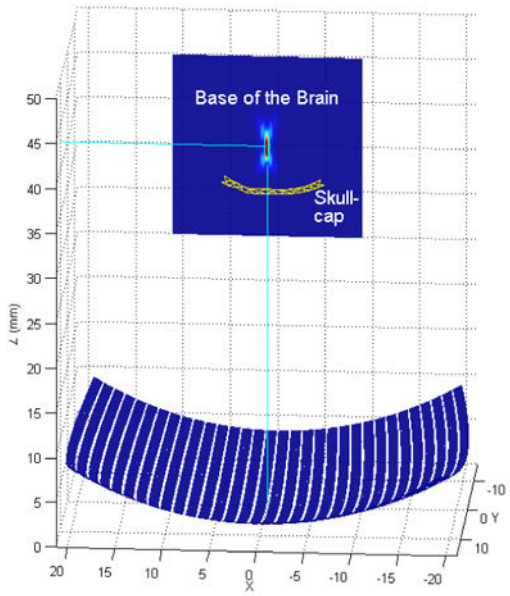

(b) DMUA schemitic representation

Fig. 1.

The DMUA prototype used in our *in vivo* and *ex vivo* experiments. The location of the skullcap is shown in (b), together with the intensity profile of the geometric focus.

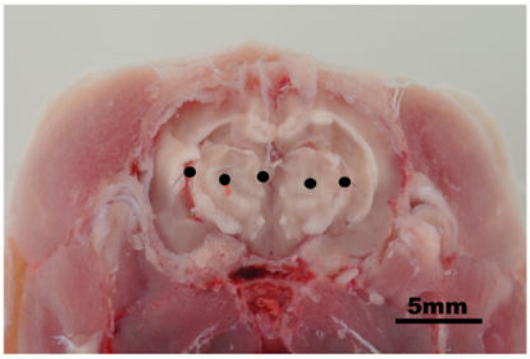

(a) Gross brain cross-section

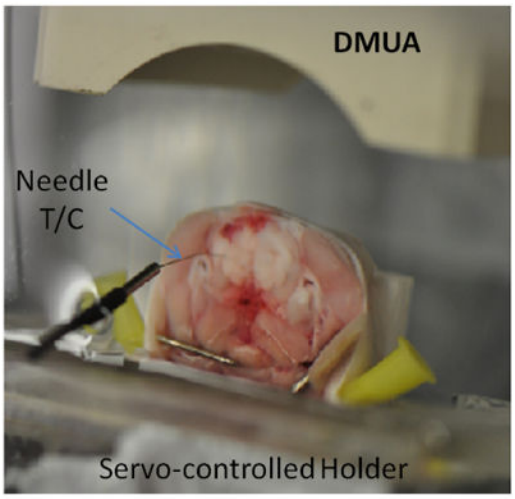

(b) Brain positioned in front of DMUA

Fig. 2.

Ex vivo imaging setup for experimental determination of the psf in synthetic-aperture DMUA imaging (a) and for direct measurement of tFUS-induced temperature using needle T/C (b).

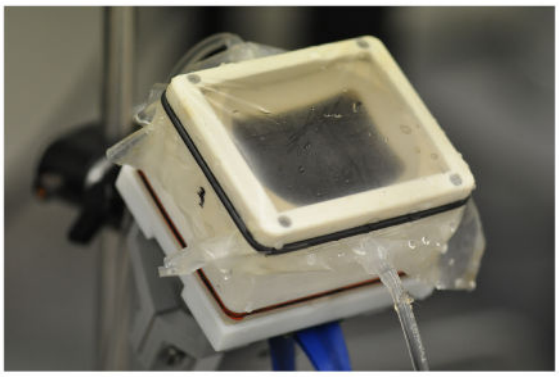

(a) DMUA encapsulated inside a water bolus.

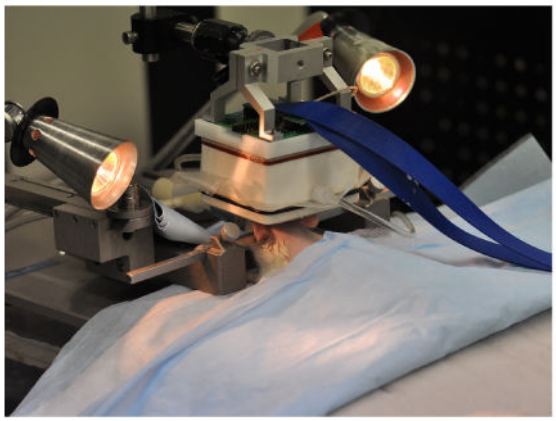

(b) Rat positioned for transcranial treatment.

Fig. 3.
Transcranial DMUA imaging and subtherapeutic heating *in vivo*.

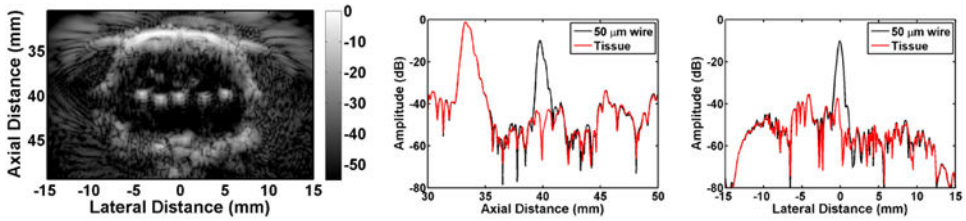

(a) SA image of brain cross-section (b) Axial profile through the skull (c) Lateral profile through the skull

Fig. 4.
Results of transcranial PSF measurements in rat brain.

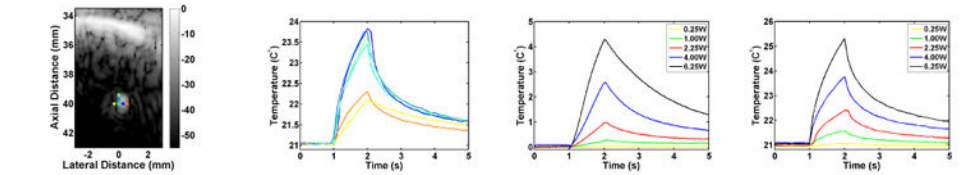

(a) Six spatial heating locations (b) Thermocouple temperature for locations in (a) (c) STF-based UST (d) Thermocouple temperature

Fig. 5.

DMUA tFUS heating in the vicinity of a thermocouple: (a) SA image with six tFUS spots (0.3 mm spacing), (b) T/C measurements at dot corresponding to tFUS spot locations, (c)& (d) temperature profiles obtained using UST and T/C measurement (at blue dot).

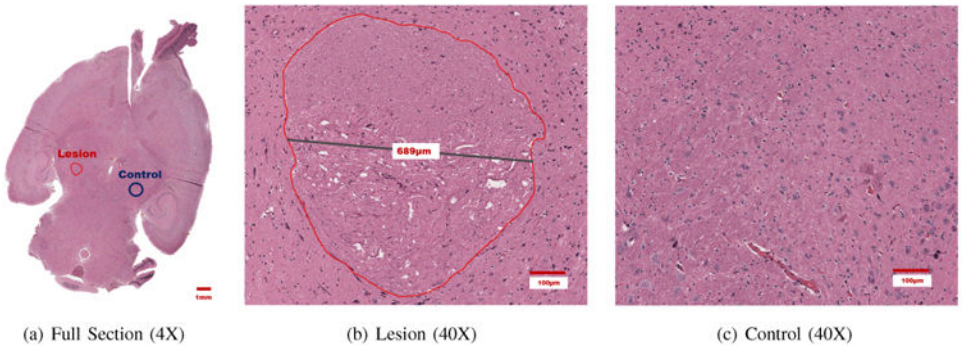

Fig. 6.

Thermal Lesion formed using DMUA tFUS beam in the left hemisphere with clear demarcation between HIFU-treated and untreated tissue.

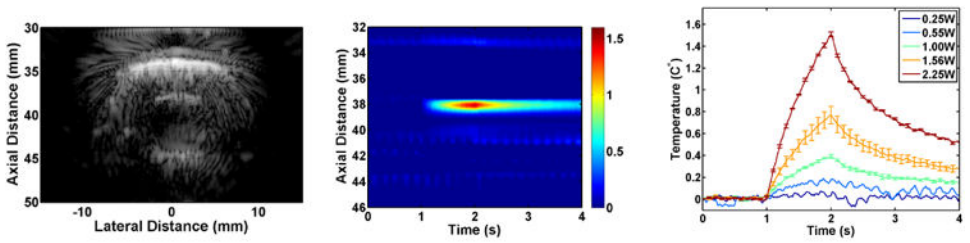

(a) Rat A: SA image (b) Rat A: Axial-temporal Temperature (c) Rat A: Temperature

Fig. 7.
Results of *in vivo* subtherapeutic tFUS application in Rat A.

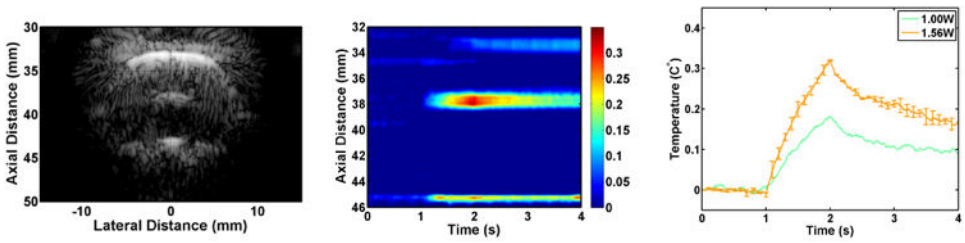

(a) Rat B: SA image (b) Rat B: Axial-temporal Temperature (c) Rat B: Temperature

Fig. 8.

Results of *in vivo* subtherapeutic tFUS application in Rat B.

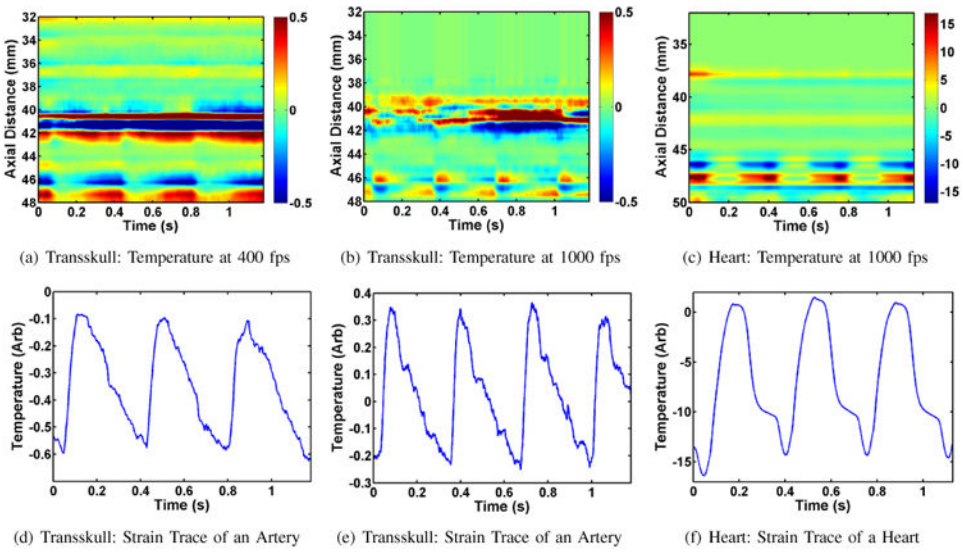

(a) Transskull: Temperature at 400 fps (b) Transskull: Temperature at 1000 fps (c) Heart: Temperature at 1000 fps

(d) Transskull: Strain Trace of an Artery (e) Transskull: Strain Trace of an Artery (f) Heart: Strain Trace of a Heart

Fig. 9.

Pulsation data recorded in Rat B; transskull imaging was done for (a), (b), (d), and (e); imaging of the heart was performed for (c) and (f).

Table I

Spatial Resolution of a 50μm Wire Embedded within Brain Tissue.

Resolution	**L1**	**L2**	**L3**	**L4**	**L5**
Axial (μm)	440	510	480	340	440
Lateral (μm)	560	640	553	462	495